

Unidimensional continuous-variable measurement-device-independent quantum key distribution

Dongyun Bai · Peng Huang · Yiqun
Zhu · Hongxin Ma · Tailong Xiao · Tao
Wang · Guihua Zeng

January 27, 2022

Abstract Continuous-variable (CV) measurement-device-independent (MDI) quantum key distribution (QKD) is immune to imperfect detection devices, which can eliminate all kinds of attacks on practical detectors. Here we first propose a CV-MDI QKD scheme using unidimensional modulation (UD) in general phase-sensitive channels. The UD CV-MDI QKD protocol is implemented with the Gaussian modulation of a single quadrature of the coherent states prepared by two legitimate senders, aiming to simplify the implementation compared with the standard, symmetrically Gaussian-modulated CV-MDI QKD protocol. Our scheme reduces the complexity of the system since it ignores the requirement in one of the quadrature modulations as well as the corresponding parameter estimations. The security of our proposed scheme is analyzed against collective attacks, and the finite-size analysis under realistic conditions is taken into account. UD CV-MDI QKD shows a comparable performance to that of its symmetrical counterpart, which will facilitate the simplification and practical implementation of the CV-MDI QKD protocols.

Keywords Unidimensional modulation · Continuous variable · Measurement-device-independent · Quantum key distribution · Finite-size analysis

Corresponding author: huang.peng@sjtu.edu.cn

Corresponding author: zhuyiq@sdju.edu.cn

Dongyun Bai

State Key Laboratory of Advanced Optical Communication Systems and Networks, School of Physics and Astronomy, Shanghai Jiao Tong University, Shanghai 200240, China

Dongyun Bai · Peng Huang · Hongxin Ma · Tailong Xiao · Tao Wang · Guihua Zeng

State Key Laboratory of Advanced Optical Communication Systems and Networks, Center of Quantum Sensing and Information Processing, Shanghai Jiao Tong University, Shanghai 200240, China

Yiqun Zhu

School of Electronic Information, Shanghai Dianji University, Shanghai 201306, China

1 Introduction

Quantum key distribution (QKD) [1–6] is one of the most mature applications in quantum information processing and quantum cryptography technology, which guarantees the unconditional secure key distribution between two remote partners, named Alice and Bob, even with the existence of a potential eavesdropper named Eve. The unconditional security is provided by the basic physical principles of quantum mechanics [7]. Continuous-variable (CV) QKD protocols [8–12], as counterparts of the discrete-variable (DV) protocols [13–15] where key information is encoded on the properties of single photons, have emerged advantages in high secret key rates and superior compatibility with practical optical systems. CV-QKD protocols can be implemented with the Gaussian modulation of the field quadratures of coherent states or squeezed states of light [16, 17]. In the last two decades, researches on CV-QKD have gradually matured [18]. In theory, Gaussian-modulated coherent-state (GMCS) CV-QKD protocols have been proved to be secure under collective attacks [19, 20] and coherent attacks [21, 22], even with finite-size regime [23, 24] and composable security [25] taken into full analysis. Numerous experimental realizations in the laboratory [26–29] and several field tests [30–32] have been achieved, which show the feasibility and practicability of CV-QKD protocols. A recent experiment of all-fiber GMCS CV-QKD has achieved the secure transmission distance beyond 100 km under laboratory conditions, which will contribute to the realization of metropolitan quantum networks with conventional telecom technologies [33].

Theoretically, the CV-QKD protocols with Gaussian modulation have been proved to be unconditionally secure under some ideal assumptions. However, in practical implementations, imperfect devices especially practical detectors may lead to some potential loopholes [34], which will further hinder the development of CV-QKD protocols. More recently, quantum attack strategies against practical detection such as local oscillator (LO) fluctuation attack [35], LO calibration attack [36], saturation attack [37] and homodyne-detector-blinding attack [38], will seriously deteriorate the actual performance of the practical quantum communication systems. One natural solution is to find a counterpart to every specific loophole, while it cannot prevent an unknown attack effectively and will greatly increase the complexity of physical implementation. To effectively fill the gap between the ideal assumptions and practical implementations, measurement-device-independent (MDI) QKD protocols were first proposed by two groups independently [39, 40], which are immune to all side-channel attacks against detectors. Inspired by the CV entanglement swapping, the MDI framework was extended to CV systems later [41–43]. CV-MDI QKD was theoretically introduced in detail with free-space experimental proofs in Ref [41]. In most CV-MDI QKD protocols, both Alice and Bob are legitimate senders, and they perform symmetrical Gaussian modulations on amplitude and phase quadratures of coherent states. Then they send their quantum states to an untrusted third party named Charlie, who performs Bell-state measurement (BSM) and then communicates the results to establish a secure key.

Since the detection is carried out by the untrusted third party, the quantum attacks related to detectors will naturally be removed, which shows the high practical security of CV-MDI QKD protocols. Till now, several tremendous results [44–49] have been obtained under the theoretical framework of CV-MDI QKD, with finite-size analysis [50, 51] and composable security analysis [52] fully accomplished.

A further simplified unidimensional modulation (UD) CV-QKD protocol has been proposed to reduce the system complexity and the cost of the apparatus [53], which thereby facilitate the commercialization of practical CVQKD schemes. Compared to the conventional symmetrical GMCS CV-QKD protocols, the asymmetrical UDCV-QKD protocols only requires the sender to use one simple modulator to perform a single-quadrature modulation instead of two modulators, which would even avoid to create a *hole* in the center of the Gaussian probability distribution [53]. Moreover, the security analysis [54–56] and several experimental realizations [57] were carried out to validate the feasibility of UDCV-QKD protocols.

So far, in all presented CV-MDI QKD protocols [41, 43], two senders both propose a symmetrical modulation by using amplitude and phase modulators, which causes the CV-MDI QKD protocols relatively complex. In order to reduce the complexity of CV-MDI QKD protocols, in this paper we extend the idea of UD to CV-MDI QKD framework, and we firstly propose a CV-MDI QKD protocol based on unidimensional modulation. In this renewed scheme, both Alice and Bob use one modulator to finish the single-quadrature modulation, then they send their prepared quantum states to Charlie for BSM. We analyze the security in a general phase-sensitive Gaussian channel under optimal collective attacks [53]. Under the physicality constraints and rational parameters related to unmodulated quadrature, we obtain the secret key rates in our UD CV-MDI QKD protocol. We also take the finite-size effects into our security analysis to obtain a tight bound under practical conditions.

The paper is structured as follows. In Sect. 2, we first review the original UD CV-QKD structure and the illustration of symmetrical modulated CV-MDI QKD protocols. In Sect. 3, we derive the secret key rate of the UD CV-MDI QKD protocol in asymptotic case, in comparisons with the conventional, symmetrical modulated CV-MDI QKD protocols. The finite-size analysis is fully taken into account in Sect. 4. Finally the conclusions and discussions are drawn in Sect. 5.

2 CV-MDI QKD protocol with unidimensional modulation

In this section, we first review the UDCV-QKD protocol and the original CV-MDI QKD protocol with symmetrical modulation. Then we introduce our proposed UD CV-MDI QKD protocol with the equivalent entanglement-based (EB) scheme presented in detail, which is more convenient and reasonable to perform the security analysis.

2.1 UDCV-QKD protocol and original CV-MDI QKD protocol

The schematic of UDCV-QKD protocol is displayed in Fig. 1(a). In prepare-and-measure (PM) model, the trusted sender Alice modulates one quadrature (amplitude quadrature \hat{x} or phase quadrature \hat{p}) of the coherent states (generated from a laser source) with modulation variance V_m by one single modulator M and then she distributes the quantum states to the remote trusted party Bob. Bob implements homodyne detection to detect the modulated quadrature. Alice and Bob use reverse reconciliation to extract secret keys by data post-processing method. Without loss of generality, in the rest of our paper, we further assume that the senders modulate the amplitude quadrature \hat{x} . The quantum channel is characterized as a phase-sensitive channel, with transmittance $\eta_{x,p}$ and excess noise $\epsilon_{x,p}$ in \hat{x} and \hat{p} quadratures respectively. It should be noted that the receiver needs to measure the other unmodulated quadrature \hat{p} sometimes to acquire the necessary properties of the channel in \hat{p} quadrature. In EB model, Alice measures one half mode of a two-mode squeezed vacuum state (TMSVS) with variance V by homodyne detection, while the other half mode is squeezed by the squeezer S and then it's projected into a coherent state and sent to the quantum channel [53, 57] to extract a secret key.

Figure 1(b) shows the PM version of the conventional CV-MDI QKD protocol [41]. The main procedures can be briefly described in the following ways: (1) Both Alice and Bob prepare the quantum states independently with symmetrical Gaussian modulation on amplitude and phase quadratures. Then the prepared quantum states are sent to the untrusted third party Charlie through two independent quantum links. (2) Charlie performs BSM on the incoming modes by interfering them on a balanced beam splitter (BS). The two output modes from BS are measured by two homodyne detectors, with the results of \hat{X} and \hat{P} announced publicly. (3) Alice and Bob use the measurement results to modify their data and then to establish a string of raw keys. (4) Alice and Bob implement parameter estimation, information reconciliation and privacy amplification to finally obtain a string of secret keys.

2.2 CV-MDI QKD with unidimensional modulation

In this part, we come to the implementation of CV-MDI QKD protocol with unidimensional modulation based on its equivalent EB version as illustrated in Fig. 2(a), for the convenience of security analysis. First we consider the state preparation at Alice's side, where a TMSVS with variance V is prepared (EPR state). One mode of the EPR state is squeezed by a squeezing operation S with a squeezing parameter $-\log\sqrt{V}$, while the other half mode A_1 is measured by Alice using homodyne detection. Then mode A_2 is conditionally prepared in coherent states with modulation variance $V_m = V^2 - 1$ and sent to Charlie. Similarly, Bob performs the same unidimensional modulation and sends mode B_2 to Charlie. Mode A' and mode B' are interfered at a balanced BS at Charlie's side. Under the previous and agreed assumption that

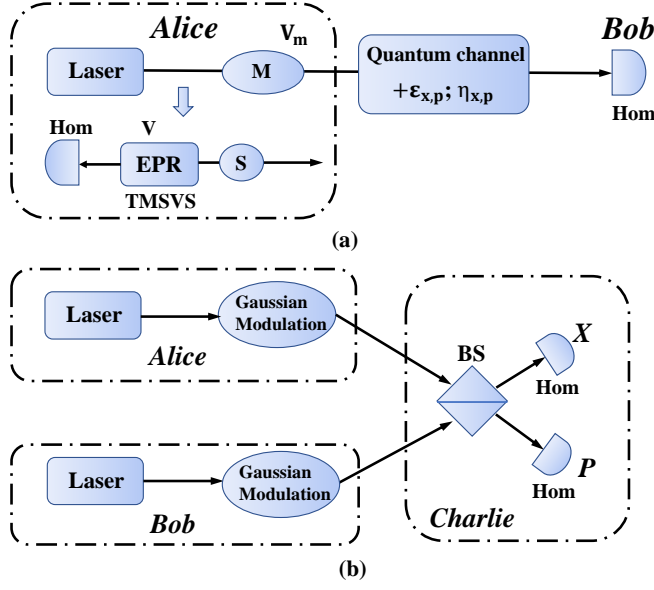


Fig. 1 (a) The prepare-and-measure (PM) model and equivalent EB model of general UDCV-QKD protocol. (b) PM model of original CV-MDI QKD protocol. M: one single modulator; S: squeezer; EPR: Einstein-Podolsky-Rosen state; TMSVS: two-mode squeezed vacuum state; Hom: homodyne detection; BS: beam splitter.

the single modulated quadrature is amplitude quadrature, Charlie announces the \hat{x} quadrature of C publicly. After receiving the measurement results of Charlie, Bob displaces mode B_1 through displacement operation D_β and gets $\hat{\rho}_{B'_1} = D_\beta \hat{\rho}_{B_1} D_\beta^\dagger$, where $\hat{\rho}$ represents the density matrix operator while β is related to the gain of displacement of Charlie's measurement results, and Alice keeps her measured data unchanged. Finally, Alice and Bob use an authenticated channel for parameter estimation, reverse reconciliation and privacy amplification to obtain a string of secure keys.

Here are two points needed to emphasize. One point is that after Charlie's measurements and Bob's displacement, mode A_1 and mode B'_1 can be treated entangled and their data is then correlated [43]. The other point is that Alice and Bob ought to sometimes switch \hat{X} and \hat{P} basis and modulate the phase quadrature \hat{p} , then Charlie needs to reveal the interference results of P_D of D sometimes for both senders to gather essential channel properties in quadrature \hat{p} [53, 55].

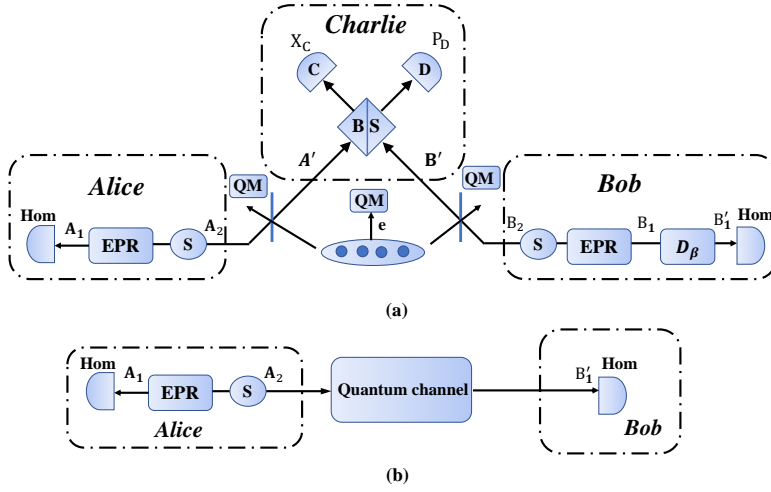


Fig. 2 (a) The equivalent EB version of CV-MDI QKD with unidimensional modulation. (b) Simplified equivalent one-way protocol of CV-MDI QKD protocol with unidimensional modulation. M: one single modulator; S: squeezer; EPR: Einstein-Podolsky-Rosen state; Hom: homodyne detection; BS: beam splitter; QM: quantum memory. D_β is displacement operation.

3 Secret key calculation with performance analysis under asymptotic case

3.1 Secret key calculation

In this section, we mainly carry out the secret key rate analysis under Gaussian collective attacks for they are proved to be optimal in asymptotic case. We derive secret key rate based on the EB scheme in Fig. 2(a). When the EPR state at Bob's side and the displacement D_β are accessible to Eve, the EB scheme in Fig. 2(a) can be conveniently equivalent to a common one-way UDCV-QKD protocol [43] shown in Fig. 2(b). For the equivalent one-way model requires more constraints on Eve, it is obvious the secret key rate in Fig. 2(b) is a lower bound of that derived from Fig. 2(a). To facilitate the calculation process with covariance matrix, we use the model in Fig. 2(b) to obtain our K_{UD} under collective attacks.

The CV-MDI QKD protocol has two quantum channels and there exists two main eavesdropping strategies: one-mode attack and two-mode attack. In practice, it's challenging for Eve to obtain quantum correlations from both channels due to technical constraints. In our work, we restrict our channels to two independent Gaussian Markovian memoryless channels, where Eve can fully implement one-mode attack. However, we should point out that Eve's attack assumed here is not as optimal as two-mode attack in Ref [41].

Generally, the lower bound of the secret key rate in Fig. 2(b) under optimal collective attack can be given as

$$\begin{aligned} K_{UD} &= \beta I_{A_1 B'_1} - \chi_E \\ &= \beta I_{A_1 B'_1} - (S(E) - S(E|X_{B'_1})). \end{aligned} \quad (1)$$

where β is the reconciliation efficiency, $I_{A_1 B'_1}$ is the Shannon mutual information between Alice and Bob with χ_E the Holevo bound between Bob and Eve, S represents the Von Neumann entropy. Since Eve could purify the whole system after Bob performs homodyne detection, thus the mutual information between Bob and Eve can be expressed as $\chi_E = S(A_1 B'_1) - S(A_1 | X_{B'_1})$.

In our UD CV-MDI QKD protocol, we focus on the modulation of \hat{x} quadrature, which results in asymmetrical covariance matrix compared with its symmetrical Gaussian modulation CV-QKD protocol. We assume that Alice and Bob use the same modulation variance V_m and the transmittance and excess noise in Alice's (Bob's) channel are $\eta_A(\eta_B)$ and $\epsilon_A(\epsilon_B)$. In the EB scheme in Fig. 2(b), Alice measures one mode of EPR state of variance V , while the other half mode is squeezed with the squeezing parameter $-\log\sqrt{V}$, which results the covariance matrix as:

$$\gamma_{A_1 A_2} = \begin{pmatrix} V & 0 & \sqrt{V(V^2-1)} & 0 \\ 0 & V & 0 & -\sqrt{\frac{V^2-1}{V}} \\ \sqrt{V(V^2-1)} & 0 & V^2 & 0 \\ 0 & -\sqrt{\frac{V^2-1}{V}} & 0 & 1 \end{pmatrix}. \quad (2)$$

Then the EB scheme is equivalent to modulate the quadrature \hat{x} with modulation variance $V_m = V^2 - 1$. After the prepared states are sent to Bob through the quantum channel with transmittance $\eta_{x,p}$ and excess noise $\epsilon_{x,p}$, the covariance matrix $\gamma_{A_1 A_2}$ is transformed into covariance matrix $\gamma_{A_1 B'_1}$ in the following form assuming perfect homodyne detection:

$$\begin{pmatrix} V & 0 & \sqrt{T_{A,x}}\sqrt{V(V^2-1)} & 0 \\ 0 & V & 0 & -\sqrt{T_{A,p}}\sqrt{\frac{V^2-1}{V}} \\ \sqrt{T_{A,x}}\sqrt{V(V^2-1)} & 0 & T_{A,x}(V^2-1+\epsilon'_{A,x})+1 & 0 \\ 0 & -\sqrt{T_{A,p}}\sqrt{\frac{V^2-1}{V}} & 0 & 1+T_{A,p}\epsilon'_{A,p} \end{pmatrix} \quad (3)$$

where $V = \sqrt{V_m + 1}$, $T_{A,x}$ and ϵ'_x correspond to Alice's channel estimated parameters in \hat{x} quadrature, and they are given as:

$$T_{A,x} = \frac{\eta_{A,x}}{2} g^2, \quad (4)$$

while

$$\begin{aligned} \epsilon'_{A,x} &= 1 + \frac{\eta_{B,x}}{\eta_{A,x}}(\chi_{B,x} - 1) + \chi_{A,x} \\ &\quad + \frac{1}{\eta_{A,x}} \left(\frac{\sqrt{2V_m}}{g} - \sqrt{\eta_B(V_m + 2)} \right)^2, \end{aligned} \quad (5)$$

with $\chi_{A,x} = \frac{1-\eta_{A,x}}{\eta_{A,x}} + \epsilon_{A,x}$, $\chi_{B,x} = \frac{1-\eta_{B,x}}{\eta_{B,x}} + \epsilon_{B,x}$, g is the gain of the displacement D_β in Bob's side. To minimize the excess noise $\epsilon'_{A,x}$, we choose $g^2 = \frac{2V_m}{\eta_{B,x}(V_m+2)}$ and derive:

$$\epsilon'_{A,x} = \epsilon_{A,x} + \frac{2}{\eta_{A,x}} + \frac{\eta_{B,x}}{\eta_{A,x}}(\epsilon_{B,x} - 2). \quad (6)$$

While $T_{A,p}$ and $\epsilon'_{A,p}$ is correlated with the \hat{p} quadrature. Theoretically, before we derive the explicit expressions of the parameters, we have to consider the relationship of the two unknown parameters $\eta_{A,p}$ and $\epsilon_{A,p}$ in \hat{p} quadrature. Bounded by the Heisenberg uncertainty principle to meet the requirement of physicality, the two unknown parameters should satisfy the parabolic equation constraint [56]:

$$\left(\sqrt{\frac{\eta_{A,x}}{(1+\eta_{A,x}\epsilon_{A,x})^2}} - \sqrt{\eta_{A,p}}\right)^2 \leq \left(1 - \frac{\eta_{A,x}}{1+\eta_{A,x}\epsilon_{A,x}}\right)\left(1 + \eta_{A,p}\epsilon_{A,p} - \frac{1}{\eta_{A,x}\epsilon_{A,x}}\right). \quad (7)$$

In Fig. 3 we explore the regions bounded by physicality with a series of parameters $\eta_{A,x}$ and $\epsilon_{A,x}$. The region is divided into three regions by every curve and on the top part separated by every individual curve, it belongs to the physical region, which means the two unknown parameters can be physically set simultaneously, otherwise the other parts will violate Heisenberg uncertainty. In typical communication channels, one always expect the values of channel loss and excess noise in both \hat{X} and \hat{P} quadratures are symmetric, and therefore we assume $\eta_{A,p} = \eta_{A,x}$ ($\eta_{B,p} = \eta_{B,x}$) and $\epsilon_{A,p} = \epsilon_{A,x}$ ($\epsilon_{B,p} = \epsilon_{B,x}$) in the rest of our paper to carry out secret key calculation [53,54]. From Fig. 3 we can prove our assumption strictly satisfy the physicality to perform unidimensional modulation and now we start to calculate the secret key rate.

The Shannon mutual information between Alice and Bob $I_{A_1 B'_1}$ can be denoted as:

$$I_{A_1 B'_1} = \frac{1}{2} \log_2 \frac{V_{A_1}}{V_{A_1|X_{B'_1}}}. \quad (8)$$

where V_{A_1} is the variance of mode A_1 , and $V_{A_1|X_{B'_1}}$ can be derived from the matrix $\gamma_{A_1|X_{B'_1}}$, which is calculated as [58]:

$$\gamma_{A_1|X_{B'_1}} = \gamma_{A_1} - \sigma_{A_1 B'_1}^T (X \gamma_{B'_1} X)^{\text{MP}} \sigma_{A_1 B'_1}. \quad (9)$$

where $X = \text{diag}(1, 0)$ and MP represents Moore-Penrose pseudo-inverse of a matrix. γ_{A_1} , $\gamma_{B'_1}$ and $\sigma_{A_1 B'_1}$ can all derived from the decomposition of $\gamma_{A_1 B'_1}$.

After some algebra calculation, we can obtain

$$I_{A_1 B'_1} = \frac{1}{2} \log_2 \frac{V}{V - \frac{T_{A,x} V (V^2 - 1)}{T_{A,x} (V^2 + \epsilon'_{A,x} - 1) + 1}}. \quad (10)$$

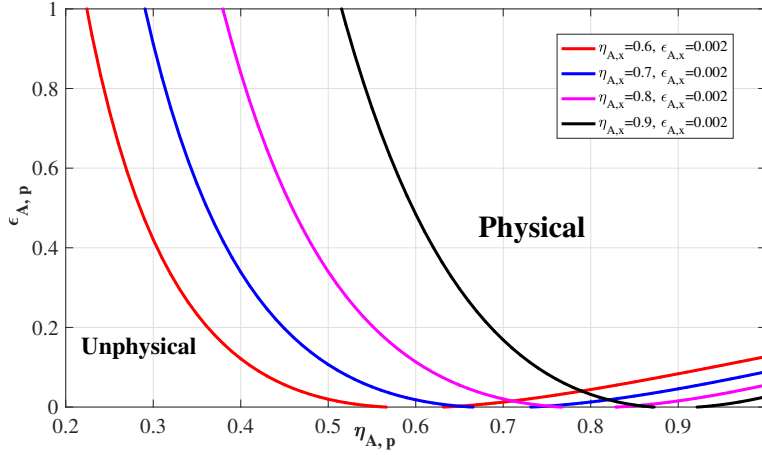


Fig. 3 Regions bounded by physicality of the varied $\eta_{A,x}$ and $\epsilon_{A,x}$. The values of these parameters can be accessible in practice.

As we have stated before, Eve can provide a purification of the whole system, so we can derive $S(E) = S(A_1 B'_1)$ and $S(E|X'_{B_1}) = S(A_1|X'_{B_1})$. $S(A_1 B'_1)$ can be written as a function of the symplectic eigenvalues $\lambda_{1,2}$ of $\gamma_{A_1 B'_1}$, denoted as

$$S(A_1 B'_1) = G(\lambda_1) + G(\lambda_2), \quad (11)$$

with

$$G(x) = \frac{(x+1)}{2} \log_2 \frac{(x+1)}{2} - \frac{(x-1)}{2} \log_2 \frac{(x-1)}{2}. \quad (12)$$

Similarly, $S(A_1|X'_{B_1})$ can be denoted as $S(A_1|X'_{B_1}) = G(\lambda_3)$, where symplectic eigenvalue λ_3 can be derived from the matrix $\gamma_{A_1|X'_{B_1}}$, considering the perfect homodyne detection at both Alice's and Bob's side.

Now we have derived all the parameters to calculate secret key rate of our UD CV-MDI QKD protocol under asymptotic case.

3.2 Performance analysis

In CV-MDI QKD protocols, there exists two different types with respect to the position of the third party Charlie. If Charlie is in the middle of Alice and Bob, we denote it as symmetric case ($L_{AC} = L_{BC}$), while if Charlie is extremely close to one party, we name it as asymmetric case ($L_{AC} \neq L_{BC}$).

At first, we analyze the secret key rate as a function of modulation variance V_m since V_m is a key parameter that will affect the performance of UD CV-MDI QKD protocol. The illustration in symmetric case is shown in Fig. 4

while the illustration in asymmetric case is shown in Fig. 5. From the two curves, we can see that in both symmetric case and asymmetric case, the large modulation could be adopted to achieve higher secret key rate, however, when the modulation is too large, the performance is not greatly improved. So considering the practical conditions, we choose the modulation variance $V_m = 100$ (in shot noise unit N_0) to calculate our secret key rate, which can lead to optimal performance.

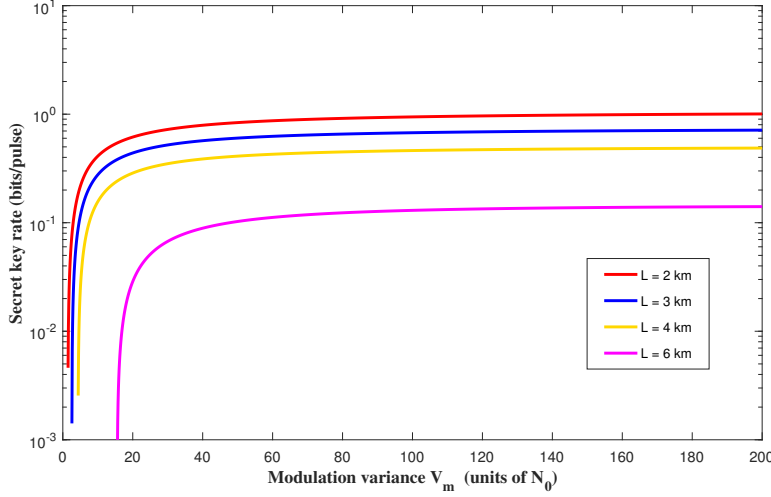


Fig. 4 Secret key rate as a function of modulation variance in symmetric case. The modulation variance V_m is in shot noise unit N_0 . The reverse reconciliation is 0.98 [56], the excess noise are $\epsilon_{A,x} = \epsilon_{B,x} = 0.002$ [44], the quantum channel loss is 0.2 dB/km. From top to bottom, the total transmission distance ($L = L_{AC} + L_{BC}$) is 2 km, 3 km, 4 km, 5 km.

The plots in Fig. 6 show secret key rate as a function of transmission distance in symmetric case, for both our UD CV-MDI QKD scheme and symmetrical Gaussian modulation CV-MDI QKD scheme. The red solid line on the left refers to the UD CV-MDI QKD protocol with $\beta = 0.96$, the blue solid line in the middle refers to the UD CV-MDI QKD protocol with $\beta = 0.98$. The dashed red line on the right represents original, symmetrical Gaussian modulation CV-MDI QKD protocol with $\beta = 0.98$, and the upper solid black line is PLOB bound, which determines the ultimate limit of repeater-less quantum communication [59]. We can see from Fig. 6 that in symmetric case, our proposed UD CV-MDI QKD scheme can achieve high performance with optimal modulation variance and the maximum transmission distance is satisfactory compared with the symmetrical CV-MDI QKD scheme.

In the asymmetric case, the plots are drawn in Fig. 7. The red solid line on the left refers to the UD CV-MDI QKD protocol with $\beta = 0.96$, the blue solid line in the middle refers to the UD CV-MDI QKD with $\beta = 0.98$. The dashed

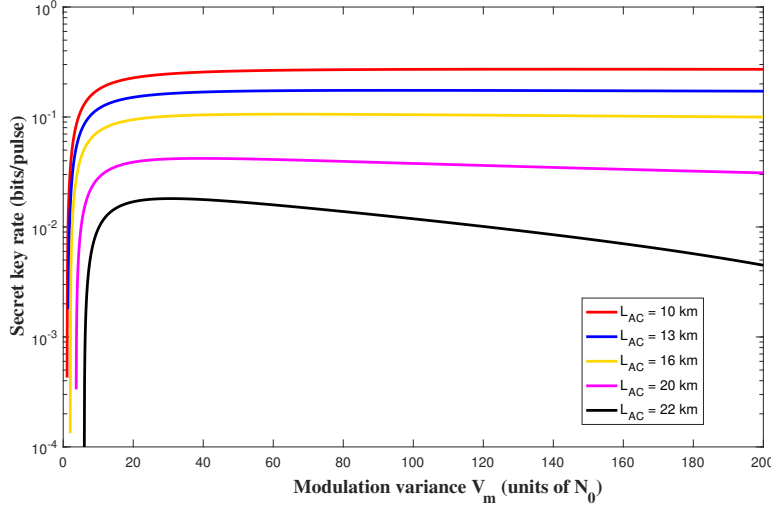


Fig. 5 Secret key rate as a function of modulation variance in asymmetric case, where Charlie is extremely close to Bob with a total efficiency 98%. The modulation variance V_m is in shot noise unit N_0 . The reverse reconciliation is 0.98, the excess noise are $\epsilon_{A,x} = \epsilon_{B,x} = 0.002$, the quantum channel loss is 0.2 dB/km. From top to bottom, the total transmission distance (L_{AC}) is 10 km, 13 km, 16 km, 20 km, 22 km.

red line on the right refers to the original, asymmetric Gaussian modulation CV-MDI QKD with $\beta = 0.98$. The PLOB bound is plotted in the solid black line. We could get from the curve that all the plots are strictly under the PLOB bound.

From Fig. 6 and Fig. 7, we can conclude that UD CV-MDI QKD in asymmetric case is superior to UD CV-MDI QKD in symmetric case, which has been proved in all the previous CV-MDI QKD schemes. In our proposed UD CV-MDI QKD protocols in both cases, the performance of our protocol is comparable to its corresponding original symmetric Gaussian modulation CV-MDI QKD protocol, while our protocols reduce the system complexity and simplify the implementation with more standard devices. In addition, UD CV-MDI QKD protocol is sensitive to reverse reconciliation efficiency especially in asymmetric case and it's reasonable for us to adopt more efficient reconciliation algorithms.

4 Finite-size analysis in UD CV-MDI QKD protocol

In the practical implementation of any CV-MDI QKD protocol, the two legitimate parties can only exchange a finite-size block of data and sacrifice part of the data for parameter estimation [24, 60]. To fill the gap between the protocol in asymptotic case and the protocol under practical conditions, we analyze the finite-size effects on our proposed UD CV-MDI QKD protocol in this section.

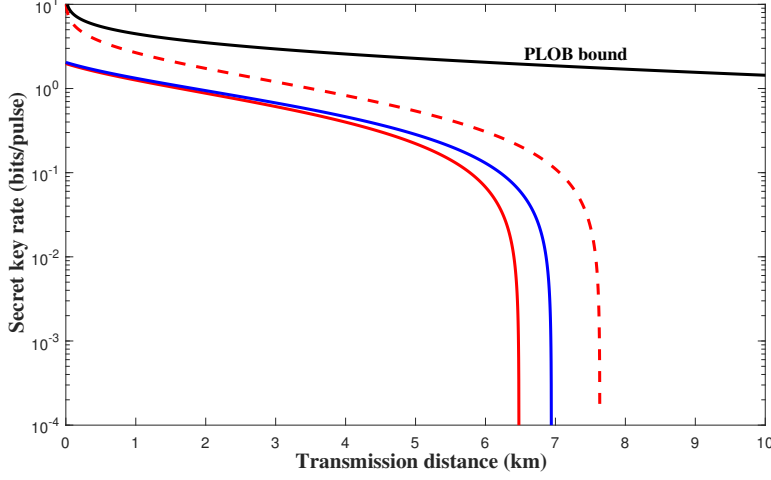


Fig. 6 Secret key rate as a function of transmission distance in symmetric case. From left to right, the red solid line represents UD CV-MDI QKD protocol with reverse reconciliation efficiency 96%, the blue solid line represents UD CV-MDI QKD protocol with reverse reconciliation efficiency 98%, while the dashed red line represents original, symmetrical Gaussian modulation CV-MDI QKD protocol with 98% efficiency. The upper solid black line is the PLOB bound. The modulation variance V_m is 100, the excess noise are $\epsilon_{A,x} = \epsilon_{B,x} = 0.002$, the quantum channel loss is 0.2 dB/km.

As all the finite-size regime did, we mainly focus on channel transmittance and excess noise within confidence intervals. To minimize the secret key rate of our protocol, we acquire the lower transmission and higher excess noise. The secret key rate in the finite-size scenario can be expressed as:

$$K_{UD}^f = \frac{n}{N} [\beta I_{A_1 B'_1} - S_{\epsilon_{PE}}(X_{B'_1}, E) - \Delta(n)]. \quad (13)$$

where N is the total number of signals exchanged between Alice and Bob, n is the number of signals used to generate secret key. The $m = N - n$ signals are used for parameter estimation. $\Delta(n)$ is the correction term related to the security of privacy amplification and has the expression

$$\Delta(n) = 7 \sqrt{\frac{\log_2(2/\tilde{\epsilon})}{n}} + \frac{2}{n} \log_2(1/\epsilon_{PA}). \quad (14)$$

with ϵ_{PA} and $\tilde{\epsilon}$ the failure probability and the smoothing parameter. Their optimal values can be conservatively set as $\epsilon_{PA} = \tilde{\epsilon} = 10^{-10}$. $I_{A_1 B'_1}$ is the mutual information of Alice and Bob, $S_{\epsilon_{PE}}(X_{B'_1}, E)$ is defined as the maximum entropy of Eve and Bob under certain failure probability ϵ_{PE} .

Now we come to the parameter estimation procedure and focus mainly on excess noise and transmittance. In practice, the estimation is sampled from m pairs of correlated variables $(x_i, p_i)_{i=1\dots m}$. Since the channel between Alice and

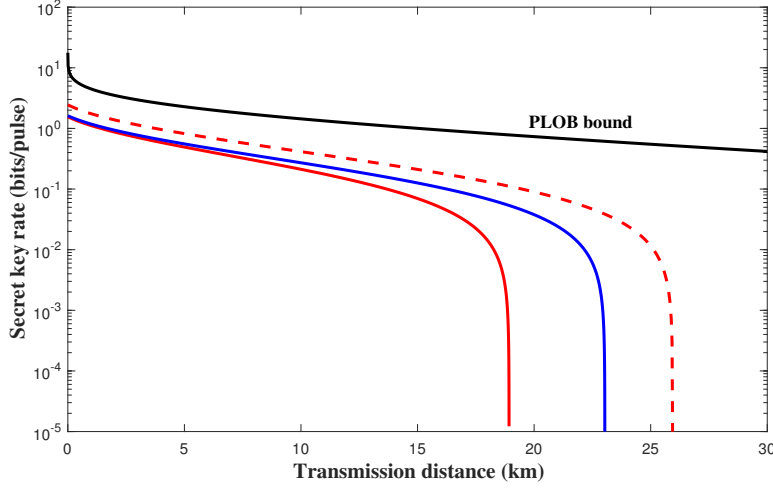


Fig. 7 Secret key rate as a function of transmission distance in asymmetric case, where Charlie is set extremely close to Bob with an overall efficiency 98%. From left to right, the red solid line represents UD CV-MDI QKD with reverse reconciliation efficiency 96%, the blue solid line represents UD CV-MDI QKD protocol with reverse reconciliation efficiency 98%, while the dashed red line represents original, symmetrical Gaussian modulation CV-MDI QKD protocol with 98% efficiency. The upper solid black line is the PLOB bound. The modulation variance V_m is 100, the excess noise are $\epsilon_{A,x} = \epsilon_{B,x} = 0.002$, the quantum channel loss is 0.2 dB/km.

Charlie, the channel between Bob and Charlie can be seen as normal linear models following Gaussian distribution. Within this model, before the BS, Alice's and Charlie's, Bob's and Charlie's data can be linked in the following relation:

$$y'_1 = t'_1 x_1 + z_1, \quad (15)$$

$$y'_2 = t'_2 x_2 + z_2, \quad (16)$$

where $t'_1 = \sqrt{\eta_{A,x}}$, $t'_2 = \sqrt{\eta_{B,x}}$. z_1 and z_2 follow a centered normal distribution with unknown variance $\sigma_1'^2 = 1 + \eta_{A,x}\epsilon_{A,x}$ and $\sigma_2'^2 = 1 + \eta_{B,x}\epsilon_{B,x}$. According to the entries of the covariance matrix, the variance of the unknown parameters before the BS can be given as:

$$\langle y_1'^2 \rangle = t_1'^2 V_m + \sigma_1'^2, \quad (17)$$

$$\langle y_2'^2 \rangle = t_2'^2 V_m + \sigma_2'^2. \quad (18)$$

Estimators $\hat{t}_1'^2$, $\hat{t}_2'^2$, $\hat{\sigma}_1'^2$ and $\hat{\sigma}_2'^2$ in maximum-likelihood analysis under the normal linear model can be expressed as:

$$\hat{t}_1' = \frac{\sum_{i=1}^m x_{1i} y'_{1i}}{\sum_{i=1}^m x_{1i}^2},$$

$$\hat{t}'_2 = \frac{\sum_{i=1}^m x_{2i} y'_{2i}}{\sum_{i=1}^m x_{2i}^2}. \quad (19)$$

$$\begin{aligned} \hat{\sigma}'_1{}^2 &= \frac{1}{m} \sum_{i=1}^m (y'_{1i} - \hat{t}'_1 x_{1i}), \\ \hat{\sigma}'_2{}^2 &= \frac{1}{m} \sum_{i=1}^m (y'_{2i} - \hat{t}'_2 x_{2i}). \end{aligned} \quad (20)$$

The independent estimators \hat{t}'_1 , \hat{t}'_2 , $\hat{\sigma}'_1{}^2$ and $\hat{\sigma}'_2{}^2$ follow the distribution below:

$$\hat{t}'_1 \sim N(t'_1, \frac{\sigma_1'^2}{\sum_{i=1}^m x_{1i}^2}), \quad \hat{t}'_2 \sim N(t'_2, \frac{\sigma_2'^2}{\sum_{i=1}^m x_{2i}^2}). \quad (21)$$

$$\frac{m\sigma_1'^2}{\sigma_1'^2}, \frac{m\sigma_2'^2}{\sigma_2'^2} \sim \chi^2(m-1). \quad (22)$$

where t'_1 , t'_2 , $\sigma_1'^2$ and $\sigma_2'^2$ are the true values of the parameters. The confidence interval of these parameters can be estimated with the except probability $\epsilon_{PE}/2$ due to the limit of m as:

$$\begin{aligned} t'_1 &\in [t'_1 - \Delta t'_1, t'_1 + \Delta t'_1], \\ t'_2 &\in [t'_2 - \Delta t'_2, t'_2 + \Delta t'_2], \\ \sigma_1'^2 &\in [\sigma_1'^2 - \Delta \sigma_1'^2, \sigma_1'^2 + \Delta \sigma_1'^2], \\ \sigma_2'^2 &\in [\sigma_2'^2 - \Delta \sigma_2'^2, \sigma_2'^2 + \Delta \sigma_2'^2]. \end{aligned} \quad (23)$$

where

$$\Delta t'_1 = z_{\epsilon_{PE}/2} \sqrt{\frac{\hat{\sigma}_1'^2}{mV_m}}, \quad \Delta t'_2 = z_{\epsilon_{PE}/2} \sqrt{\frac{\hat{\sigma}_2'^2}{mV_m}}, \quad (24)$$

$$\Delta \sigma_1'^2 = z_{\epsilon_{PE}/2} \frac{\sigma_1'^2}{\sqrt{\frac{m}{2}}}, \quad \Delta \sigma_2'^2 = z_{\epsilon_{PE}/2} \frac{\sigma_2'^2}{\sqrt{\frac{m}{2}}}. \quad (25)$$

where $z_{\epsilon_{PE}/2}$ is around 6.5 when the σ_{PE} is generally taken as 10^{-10} [23, 24]. Now we can estimate minimum $\eta_{A,x} = \hat{t}'_1{}^2$, $\eta_{B,x} = \hat{t}'_2{}^2$ and maximum $\epsilon_{A,x} = \frac{\hat{\sigma}_1'^2 - 1}{\hat{t}'_1{}^2}$, $\epsilon_{B,x} = \frac{\hat{\sigma}_2'^2 - 1}{\hat{t}'_2{}^2}$ using the previous confidence intervals and calculation results. After Charlie has finished the measurements, we can further estimate the parameters in covariance matrix $\gamma_{A_1 B'_1}$ as:

$$T_{A,x} = \frac{\eta_{A,x}}{2} g^2, \quad T_{B,x} = \frac{\eta_{B,x}}{2} g^2, \quad (26)$$

$$\epsilon'_{A,x} = \epsilon_{A,x} + \frac{2}{\eta_{A,x}} + \frac{\eta_{B,x}}{\eta_{A,x}} (\epsilon_{B,x} - 2). \quad (27)$$

where we select $g^2 = \frac{2V_m}{\eta_{B,x}(V_m+2)}$. As the parameters are all derived from the above part, now we can analyze the finite-size effects.

Figure. 8 and Fig. 9 demonstrate the secret key rate as a function of transmission distance in the symmetric case and asymmetric case considering the

finite-size effects. The data length n to generate the secret key is half of the total block length. Simulation results show that the finite-size effects will significantly influence the performance of our proposed UD CV-MDI QKD protocol with a rather small amount of data exchanged. As the number of the exchanged data increases, the performance will gradually approach the corresponding asymptotic case. In addition, the scheme is robust against the finite-size effect with the block length larger than 10^9 . In both curves, the PLOB bound is plotted and the results are strictly under the PLOB bound region. To better perform UD CV-QKD protocol, it's essential to exchange a sufficient number of block data.

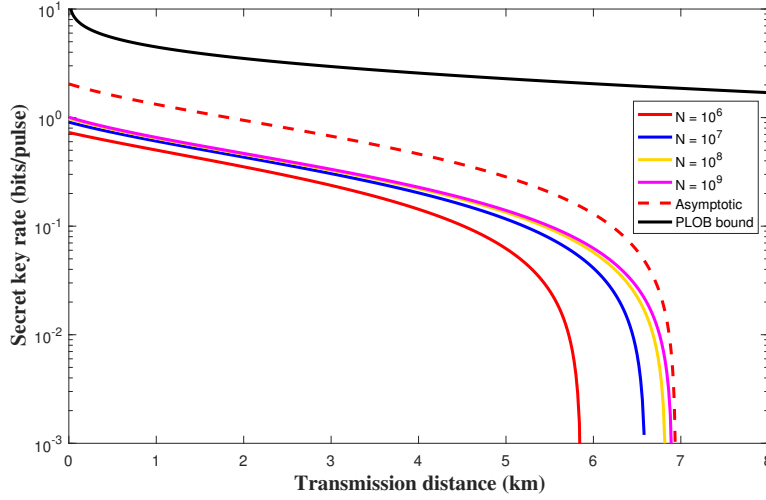


Fig. 8 Secret key rate as a function of transmission distance in symmetric case considering finite-size effects. From left to right, the block length is equal to 10^6 , 10^7 , 10^8 , 10^9 and infinite. The upper solid black line is the PLOB bound. The modulation variance V_m is 100, $\beta = 0.98$, the excess noise are $\epsilon_{A,x} = \epsilon_{B,x} = 0.002$, the quantum channel loss is 0.2 dB/km.

5 Conclusion

In this paper, we have firstly introduced a CV-MDI QKD scheme with unidimensional modulation based on the Gaussian modulation of a single quadrature of the coherent lights, which will greatly reduce the implementation complexity and allow more standard devices, as well we illustrate the physicality of the other unmodulated quadrature. Moreover, we investigate the finite-size effects under practical conditions to fill the gap between the asymptotic case and the practical case and we found that our protocol is robust to finite-size effects with large block data length (larger than 10^9). Overall, our simulation results

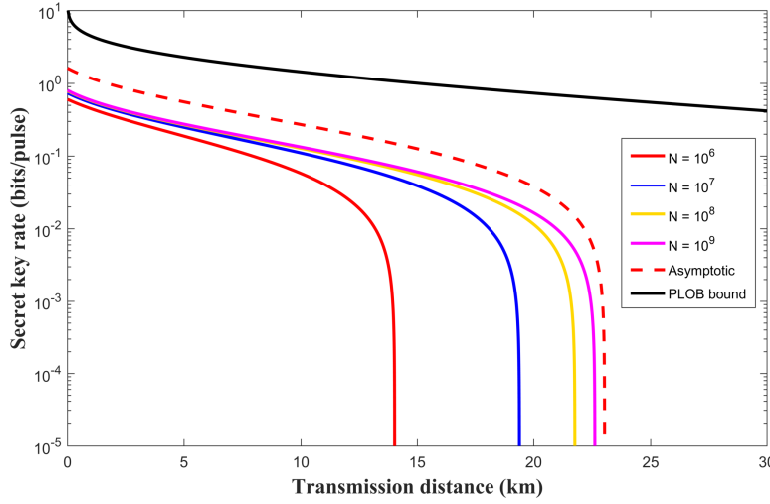


Fig. 9 Secret key rate as a function of transmission distance in asymmetric case considering finite-size effects. Where Charlie is set extremely close to Bob with an overall efficiency 0.98. From left to right, the block length is equal to 10^6 , 10^7 , 10^8 , 10^9 and infinite. The other parameters are the same as Fig. 8.

under accessible parameters show that compared with the original, symmetric Gaussian modulation protocol, our UD CV-MDI QKD protocol is still comparable to its counterpart with acceptable secret key rate and considerable system simplification.

Acknowledgements This work was supported by the National Key Research and Development Program (Grant No. 2016YFA0302600), the National Natural Science Foundation of China (Grants No. 61332019, No. 61671287, No. 61631014), and the National Key Research and Development Program of China (Grant No. 2013CB338002).

References

1. Bennett, C.H., Brassard, G.: An update on quantum cryptography. In: Workshop on the Theory and Application of Cryptographic Techniques, pp. 475–480. Springer (1984)
2. Ekert, A.: Quantum cryptography based on bell’s theorem. *Phys. Rev. Lett.* **67**(6), 661–663 (1991)
3. Gisin, N., Ribordy, G., Tittel, W., Zbinden, H.: Quantum cryptography. *Rev. Mod. Phys.* **74**(1), 145 (2002)
4. Scarani, V., Bechmannpasquinucci, H., Cerf, N., Dusek, M., Lutkenhaus, N., Peev, M.: The security of practical quantum key distribution. *Rev. Mod. Phys.* **81**(3), 1301–1350 (2009)
5. Braunstein, S.L., Van Loock, P.: Quantum information with continuous variables. *Rev. Mod. Phys.* **77**(2), 513 (2005)
6. Liao, S.K., Cai, W.Q., Liu, W.Y., Zhang, L., Li, Y., Ren, J.G., Yin, J., Shen, Q., Cao, Y., Li, Z.P.: Satellite-to-ground quantum key distribution. *Nature* **549**(7670), 43 (2017)
7. Bang, J.Y., Berger, M.S.: Quantum mechanics and the generalized uncertainty principle. *Phys. Rev. D* **74**(12), 125012 (2006)

8. Ralph, T.C.: Continuous variable quantum cryptography. *Phys. Rev. A* **61**(1), 010303 (1999)
9. Grosshans, F., Grangier, P.: Continuous variable quantum cryptography using coherent states. *Phys. Rev. Lett.* **88**(5), 057902 (2002)
10. Grosshans, F., Van Assche, G., Wenger, J., Brouri, R., Cerf, N., Grangier, P.: Quantum key distribution using gaussian-modulated coherent states. *Nature (London)* **421**(6920), 238–241 (2003)
11. Bai, D., Huang, P., Ma, H., Wang, T., Zeng, G.: Performance improvement of plug-and-play dual-phase-modulated quantum key distribution by using a noiseless amplifier. *Entropy* **19**(10), 546 (2017)
12. Liu, W., Huang, P., Peng, J., Fan, J., Zeng, G.: Integrating machine learning to achieve an automatic parameter prediction for practical continuous-variable quantum key distribution. *Phys. Rev. A* **97**(2) (2018)
13. Lo, H.K., Ma, X., Chen, K.: Decoy state quantum key distribution. *Phys. Rev. Lett.* **94**(23), 230504 (2005)
14. Xuan, Q.D., Zhang, Z., Voss, P.L.: A 24 km fiber-based discretely signaled continuous variable quantum key distribution system. *Opt. Express* **17**(26), 24244–24249 (2009)
15. Lo, H.K., Curty, M., Tamaki, K.: Secure quantum key distribution. *Nat. Photon.* **8**(8), 595 (2014)
16. Gottesman, D., Preskill, J.: Secure quantum key distribution using squeezed states. In: *Quantum Information with Continuous Variables*, pp. 317–356. Springer (2003)
17. García-Patrón, R., Cerf, N.J.: Continuous-variable quantum key distribution protocols over noisy channels. *Phys. Rev. Lett.* **102**(13), 130501 (2009)
18. Weedbrook, C., Pirandola, S., García-Patrón, R., Cerf, N., Ralph, T.C., Shapiro, J.H., Lloyd, S.: Gaussian quantum information. *Rev. Mod. Phys.* **84**(2), 621–669 (2012)
19. García-Patrón, R., Cerf, N.J.: Unconditional optimality of gaussian attacks against continuous-variable quantum key distribution. *Phys. Rev. Lett.* **97**(19), 190503 (2006)
20. Navascués, M., Grosshans, F., Acín, A.: Optimality of gaussian attacks in continuous-variable quantum cryptography. *Phys. Rev. Lett.* **97**(19), 190502 (2006)
21. Furrer, F., Franz, T., Berta, M., Leverrier, A., Scholz, V.B., Tomamichel, M., Werner, R.F.: Continuous variable quantum key distribution: finite-key analysis of composable security against coherent attacks. *Phys. Rev. Lett.* **109**(10), 100502 (2012)
22. Leverrier, A., García-Patrón, R., Renner, R., Cerf, N.J.: Security of continuous-variable quantum key distribution against general attacks. *Phys. Rev. Lett.* **110**(3), 030502 (2013)
23. Leverrier, A., Grosshans, F., Grangier, P.: Finite-size analysis of a continuous-variable quantum key distribution. *Phys. Rev. A* **81**(6), 062343 (2010)
24. Jouguet, P., Kunz-Jacques, S., Diamanti, E., Leverrier, A.: Analysis of imperfections in practical continuous-variable quantum key distribution. *Phys. Rev. A* **86**(3), 032309 (2012)
25. Leverrier, A.: Composable security proof for continuous-variable quantum key distribution with coherent states. *Phys. Rev. Lett.* **114**(7), 070501 (2015)
26. Lodewyck, J., Bloch, M., García-Patrón, R., Fossier, S., Karpov, E., Diamanti, E., Debuisschert, T., Cerf, N.J., Tualle-Brouri, R., McLaughlin, S.W., et al.: Quantum key distribution over 25 km with an all-fiber continuous-variable system. *Phys. Rev. A* **76**(4), 042305 (2007)
27. Jouguet, P., Kunzjacques, S., Leverrier, A., Grangier, P., Diamanti, E.: Experimental demonstration of long-distance continuous-variable quantum key distribution. *Nat. Photon.* **7**(5), 378–381 (2013)
28. Qi, B., Lougovski, P., Pooser, R., Grice, W., Bobrek, M.: Generating the local oscillator locally in continuous-variable quantum key distribution based on coherent detection. *Phys. Rev. X* **5**(4), 041009 (2015)
29. Wang, T., Huang, P., Zhou, Y., Liu, W., Ma, H., Wang, S., Zeng, G.: High key rate continuous-variable quantum key distribution with a real local oscillator. *Opt. Express* **26**(3), 2794–2806 (2018)
30. Fossier, S., Diamanti, E., Debuisschert, T., Villing, A., Tualle-Brouri, R., Grangier, P.: Field test of a continuous-variable quantum key distribution prototype. *New J. Phys.* **11**(4), 045023 (2009)

31. Jouguet, P., Kunz-Jacques, S., Debuisschert, T., Fossier, S., Diamanti, E., Alléaume, R., Tualle-Broui, R., Grangier, P., Leverrier, A., Pache, P., et al.: Field test of classical symmetric encryption with continuous variables quantum key distribution. *Opt. Express* **20**(13), 14030–14041 (2012)
32. Huang, D., Huang, P., Li, H., Wang, T., Zhou, Y., Zeng, G.: Field demonstration of a continuous-variable quantum key distribution network. *Opt. Lett.* **41**(15), 3511–3514 (2016)
33. Huang, D., Huang, P., Lin, D., Zeng, G.: Long-distance continuous-variable quantum key distribution by controlling excess noise. *Sci. Rep.* **6**(1), 19201–19201 (2016)
34. Gerhardt, I., Liu, Q., Lamas-Linares, A., Skaar, J., Kurtsiefer, C., Makarov, V.: Full-field implementation of a perfect eavesdropper on a quantum cryptography system. *Nat. Commun.* **2**, 349 (2011)
35. Ma, X.C., Sun, S.H., Jiang, M.S., Liang, L.M.: Local oscillator fluctuation opens a loophole for eaves in practical continuous-variable quantum-key-distribution systems. *Phys. Rev. A* **88**(2), 290–296 (2013)
36. Jouguet, P., Kunzjacques, S., Diamanti, E.: Preventing calibration attacks on the local oscillator in continuous-variable quantum key distribution. *Phys. Rev. A* **87**(6), 4996–4996 (2013)
37. Qin, H., Kumar, R., Alléaume, R.: Saturation attack on continuous-variable quantum key distribution system. In: *Emerging Technologies in Security and Defence; and Quantum Security II; and Unmanned Sensor Systems X*, vol. 8899, p. 88990N. International Society for Optics and Photonics (2013)
38. Qin, H., Kumar, R., Makarov, V., Alléaume, R.: Homodyne-detector-blinding attack in continuous-variable quantum key distribution. *Phys. Rev. A* **98**, 012312 (2018)
39. Braunstein, S.L., Pirandola, S.: Side-channel-free quantum key distribution. *Phys. Rev. Lett.* **108**(13), 130502 (2012)
40. Lo, H., Curty, M., Qi, B.: Measurement-device-independent quantum key distribution. *Phys. Rev. Lett.* **108**(13), 130503 (2012)
41. Pirandola, S., Ottaviani, C., Spedalieri, G., Weedbrook, C., Braunstein, S.L., Lloyd, S., Gehring, T., Jacobsen, C.S., Andersen, U.L.: High-rate measurement-device-independent quantum cryptography. *Nat. Photonics* **9**(6), 397–402 (2015)
42. Ma, X.C., Sun, S.H., Jiang, M.S., Gui, M., Liang, L.M.: Gaussian-modulated coherent-state measurement-device-independent quantum key distribution. *Phys. Rev. A* **89**(4), 4089–4091 (2013)
43. Li, Z., Zhang, Y., Xu, F., Peng, X., Guo, H.: Continuous-variable measurement-device-independent quantum key distribution. *Phys. Rev. A* **89**(5), 052301 (2014)
44. Ma, H.X., Huang, P., Bai, D.Y., Wang, S.Y., Bao, W.S., Zeng, G.H.: Continuous-variable measurement-device-independent quantum key distribution with photon subtraction. *Phys. Rev. A* **97**(4), 042329 (2018)
45. Zhao, Y., Zhang, Y., Xu, B., Yu, S., Guo, H.: Continuous-variable measurement-device-independent quantum key distribution with virtual photon subtraction. *Phys. Rev. A* **97**(4), 042328 (2018)
46. Wang, Y., Wang, X., Li, J., Huang, D., Zhang, L., Guo, Y.: Self-referenced continuous-variable measurement-device-independent quantum key distribution. *Phys. Lett. A* **382**(17), 1149–1156 (2018)
47. Yin, H.L., Zhu, W., Fu, Y.: Phase self-aligned continuous-variable measurement-device-independent quantum key distribution. *Sci. Rep.* **9**(1), 49 (2019)
48. Ma, H.X., Huang, P., Bai, D.Y., Wang, T., Wang, S.Y., Bao, W.S., Zeng, G.H.: Long-distance continuous-variable measurement-device-independent quantum key distribution with discrete modulation. *Phys. Rev. A* **99**(2), 022322 (2019)
49. Bai, D., Huang, P., Ma, H., Wang, T., Zeng, G.: Passive state preparation in continuous-variable measurement-device-independent quantum key distribution. *J. Phys. B* (2019)
50. Papanastasiou, P., Ottaviani, C., Pirandola, S.: Finite-size analysis of measurement-device-independent quantum cryptography with continuous variables. *Phys. Rev. A* **96**(4), 042332 (2017)
51. Zhang, X., Zhang, Y., Zhao, Y., Wang, X., Yu, S., Guo, H.: Finite-size analysis of continuous-variable measurement-device-independent quantum key distribution. *Phys. Rev. A* **96**(4), 042334 (2017)

-
52. Lupo, C., Ottaviani, C., Papanastasiou, P., Pirandola, S.: Continuous-variable measurement-device-independent quantum key distribution: Composable security against coherent attacks. *Phys. Rev. A* **97**(5), 052327 (2018)
 53. Usenko, V.C., Grosshans, F.: Unidimensional continuous-variable quantum key distribution. *Phys. Rev. A* **92**(6), 062337 (2015)
 54. Wang, P., Wang, X., Li, J., Li, Y.: Finite-size analysis of unidimensional continuous-variable quantum key distribution under realistic conditions. *Opt. Express* **25**(23), 27995–28009 (2017)
 55. Liao, Q., Guo, Y., Xie, C., Huang, D., Huang, P., Zeng, G.: Composable security of unidimensional continuous-variable quantum key distribution. *Quantum Inf. Process.* **17**(5), 113 (2018)
 56. Wang, P., Wang, X., Li, Y.: Security analysis of unidimensional continuous-variable quantum key distribution using uncertainty relations. *Entropy* **20**(3), 157 (2018)
 57. Wang, X., Liu, W., Wang, P., Li, Y.: Experimental study on all-fiber-based unidimensional continuous-variable quantum key distribution. *Phys. Rev. A* **95**(6), 062330 (2017)
 58. Fossier, S., Diamanti, E., Debuisschert, T., Tuallebrouri, R., Grangier, P.: Improvement of continuous-variable quantum key distribution systems by using optical preamplifiers. *J. Phys. B* **42**(11), 114014 (2009)
 59. Pirandola, S., Laurenza, R., Ottaviani, C., Banchi, L.: Fundamental limits of repeaterless quantum communications. *Nat. Commun.* **8**, 15043 (2017)
 60. Ruppert, L., Usenko, V.C., Filip, R.: Long-distance continuous-variable quantum key distribution with efficient channel estimation. *Phys. Rev. A* **90**(6), 062310 (2014)